Signatures of quantum spin liquid state in triangular-based zig-zag polyaromatic hydrocarbon radicals

Yongbing Shen,*[a] Mengxing Cui, [b] Haitao Zhang, [b] Hanjie Guo, [c] Jumpei G. Nakamura, [d] Jan Peter Embs, [e] Jinkui Zhao, [c,f,g] Masahiro Yamashita, *[b,h] and Zhendong Fu *[c]

[a.] Department of Chemistry, School of Science, The University of Tokyo, 7-3-1 Hongo, Bunkyo-ku, Tokyo, 113-0033, Japan.
  E-mail: shenyongbing17@gmail.com
[b.] School of Chemical Science and Engineering, Tongji University, Siping Road 1239, Shanghai 200092, P. R. China.
  E-mail: yamasita.m@gmail.com
[c.] Songshan Lake Materials Laboratory, Dongguan, Guangdong Province 523808, China.
  E-mail: zdfu@pku.edu.cn
[d.] Muon Science Laboratory, Institute of Materials Structure Science, KEK, Tokai, Ibaraki 319-1106, Japan.
[e.] Laboratory for Neutron Scattering and Imaging, Paul Scherrer Institut (PSI), CH-5232 Villigen, Switzerland.
[f.] Beijing National Laboratory for Condensed Matter Physics, Institute of Physics, Chinese Academy of Sciences, Beijing 100190, China.
[g.] School of Physical Sciences, Great Bay University, Dongguan 523808, China.
[h.] Department of Chemistry, Graduate School of Science, Tohoku University, 6-3 Aramaki-Aza-Aoba-Ku, Sendai 980-8578, Japan.

Table of contents:

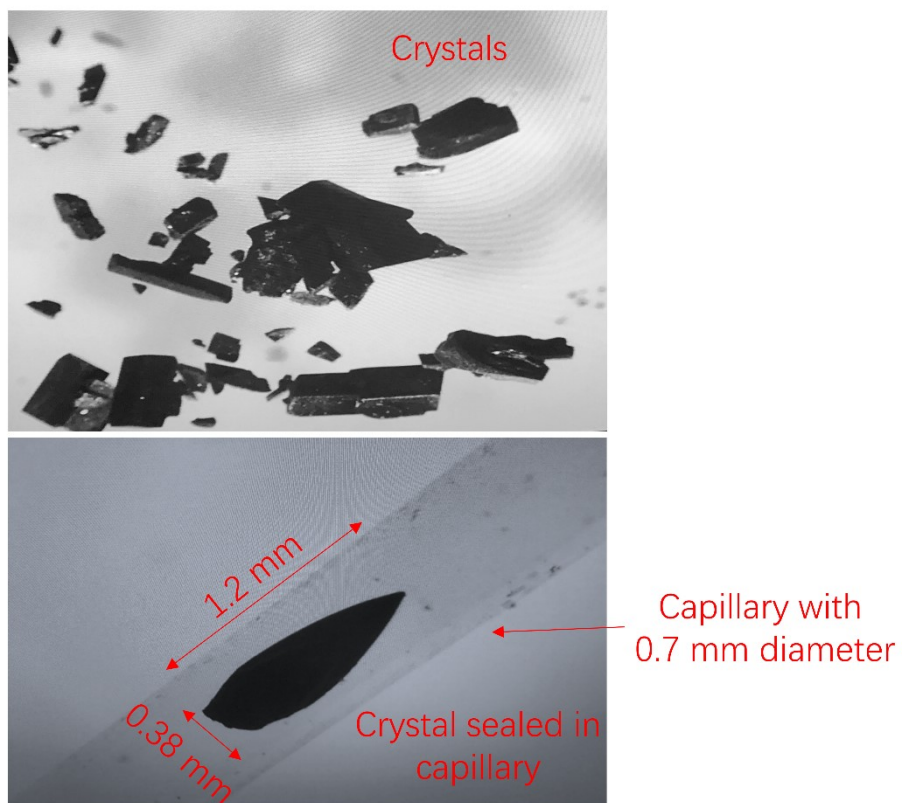Additional Notes: Inelastic neutron scattering data.

Fig. S1. The morphology of crystals of **1** (upper image). Single-crystal was inserted into the capillary and sealed with argon for structural determination (lower image).
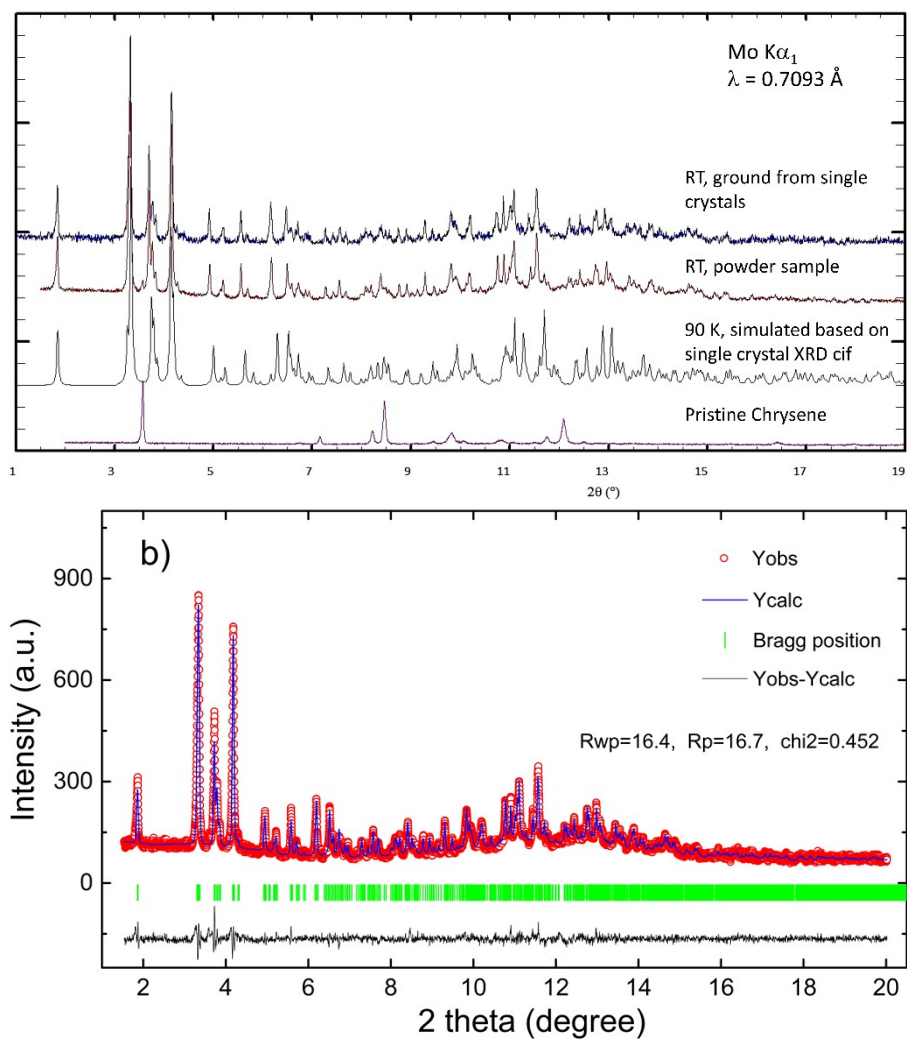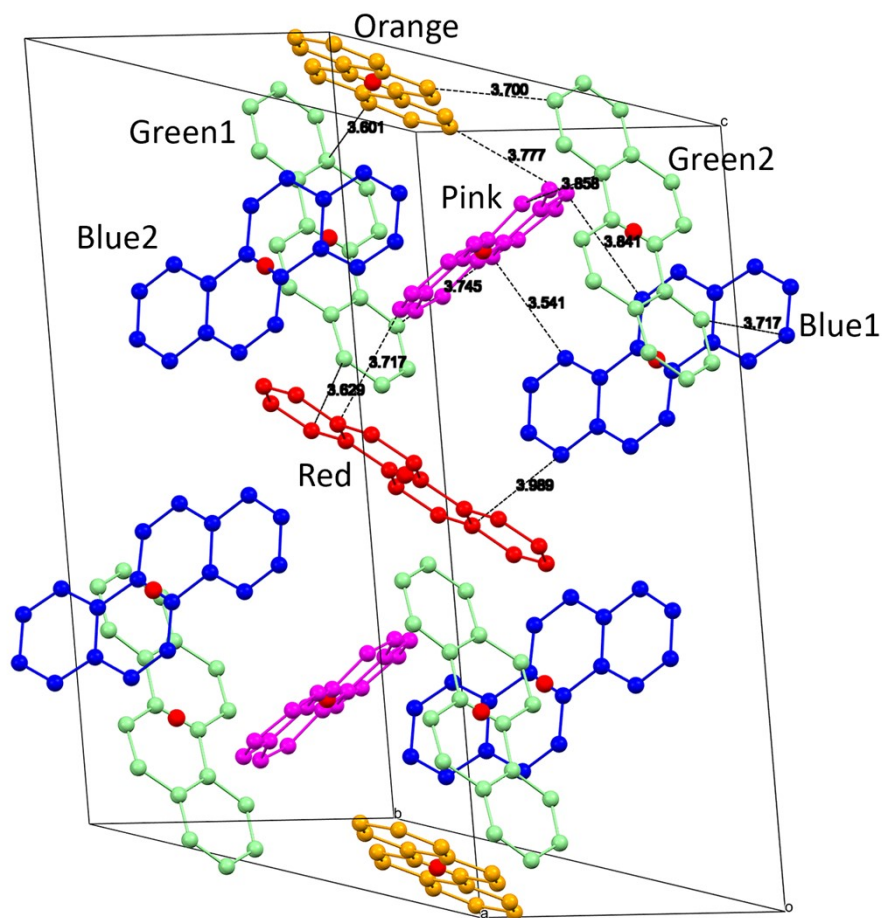
Fig. S2. a) The purity checks by comparison of experimental and simulated PXRD. **b)** The observed and calculated patterns obtained from the Rietveld analysis.
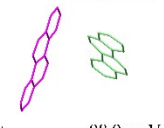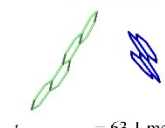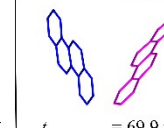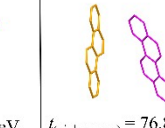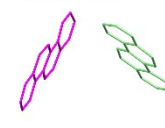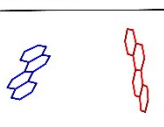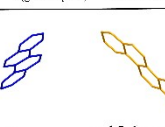
The shortest **C–C distances** between neighboring chrysene molecules:

Pink-blue1- = 3.541 Å
Pink-red = 3.717 Å
Pink-green1 = 3.745 Å
Pink-green2 = 3.858 Å
Pink-orange = 3.777 Å
Blue1-red = 3.989 Å
Red-green1= 3.629 Å
Green1-orange= 3.601 Å
Orange-green2 = 3.700 Å
Green2-blue1 = 3.717 Å

Fig. S3. The intermolecular shortest C-C distances.
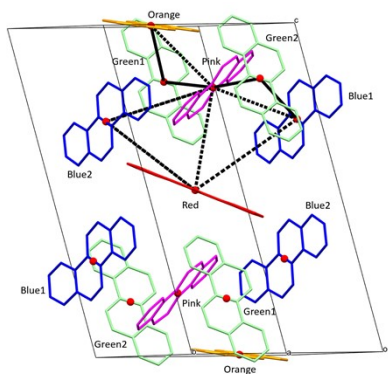
The distances between the chrysene centers are shown as:

Pink-green2= 5.948 Å	Green2-blue1= 6.307 Å
Blue1-pink= 5.855 Å	Pink-orange= 5.713 Å
Orange-green1= 7.158 Å	Green1-pink= 6.483 Å
Red-pink= 6.792 Å	
Blue2-red= 8.269 Å	Blue2-orange= 7.664 Å
Blue2-pink= 8.229 Å	Blue2-green1= 10.479 Å
Blue2-green2= 10.482 Å	Red-blue1= 8.089 Å

7 effective charge transfer integral (t)

$t_{(pink-green2)} = 98.9$ meV $t_{(green2-blue1)} = 63.1$ meV $t_{(blue1-pink)} = 69.9$ meV $t_{(pink-orange)} = 76.8$ meV

$t_{(orange-green1)} = 67.7$ meV $t_{(green1-pink)} = 76.6$ meV $t_{(red-pink)} = 76.6$ meV

6 negligible charge transfer integral (t)

$t_{(blue2-red)} = 16.2$ meV $t_{(blue2-orange)} = 15.6$ meV $t_{(blue2-pink)} = 18.7$ meV

$t_{(blue2-green1)} = 14.3$ meV $t_{(blue2-green2)} = 13.5$ meV $t_{(red-blue1)} = 26.2$ meV

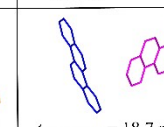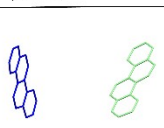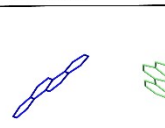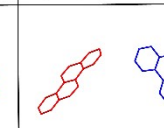| Compound 1	types	LUMO (eV)	LUMO+1 (eV)	t(electron) (eV)
7 effective t	Pink-orange	-1.8177	-1.6641	0.0768
	Blue1-pink	-1.8093	-1.6695	0.0699
	pink-green2	-1.8553	-1.6575	0.0989
	Red-pink	-1.8305	-1.6773	0.0766
	Green1-pink	-1.8305	-1.6773	0.0766
	Green2-blue1	-1.8121	-1.6858	0.0631
	Orange-green1	-1.8077	-1.6723	0.0677
6 negligible t	Blue2-red-1	-1.7884	-1.7560	0.0162
	Blue1-red-6	-1.8232	-1.7709	0.0262
	Blue2-pink-3	-1.8098	-1.7724	0.0187
	Blue2-orange-2	-1.8021	-1.7709	0.0156
	Blue2-green1	-1.7758	-1.7472	0.0143
	Blue2-green2	-1.7927	-1.7657	0.0135

Fig. S4. The distances between the chrysene centers and the 13 possibilities of charge transfer integrals calculations.
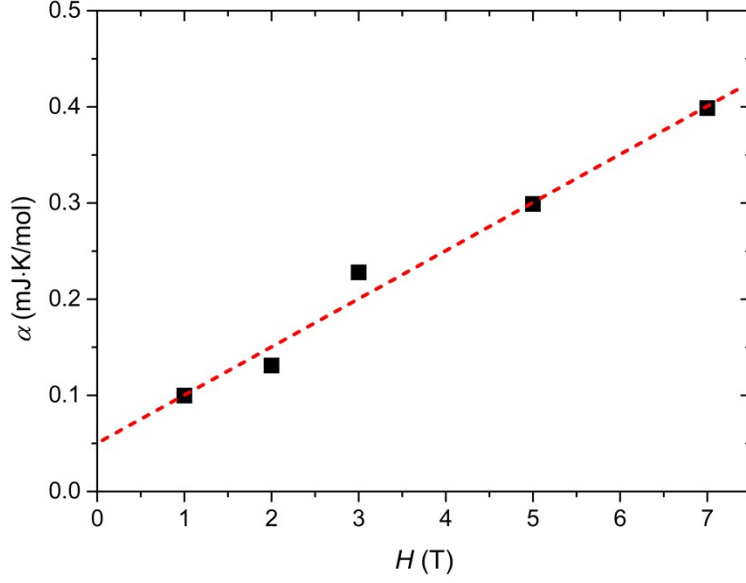
Fig. S5. Field dependence of α, together with the linear fit and the extrapolation to H = 0. The upturn of the specific heat at the lowest temperatures is caused by the hyperfine splitting of the nuclear energy levels and can be described as the high-T tail of a Schottky anomaly, $C_{hyp} = \alpha T^{-2}$. α is determined by fitting the data measured under external fields and plotted against H. The red dash line is the linear fit to the field dependence of α, whose extrapolation yields $\alpha = 0.050(17)$ mJ·K/mol at $H = 0$, in reasonable agreement with the Schottky contributions from hydrogen nuclear spins in the QSL candidates, $ZnCu_3(OH)_6SO_4$ and κ-$(BEDT\text{-}TTF)_2Cu_2(CN)_3$.[3,4] Therefore we attribute the upturn below 0.3 K to the Schottky contribution of hydrogen nuclear spins.
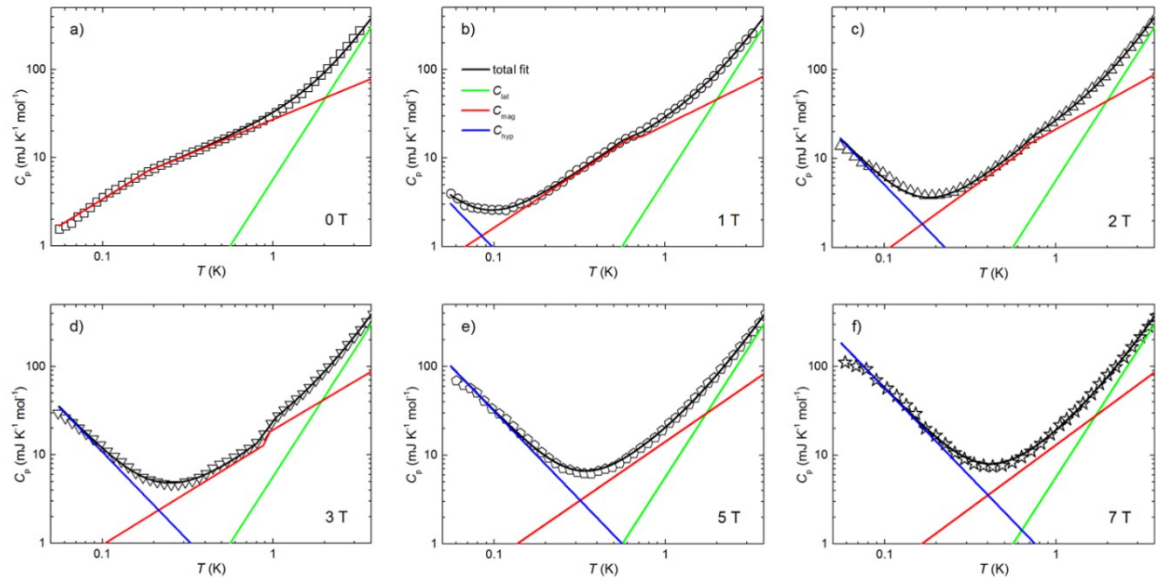
Fig. S6. Specific heat data for various external fields with best fits. The specific heat data for various external fields are plotted along with the best total fits (black lines), the lattice contribution C_{lat} (green lines), the hyperfine contribution C_{hyp} (blue lines), and the magnetic contribution C_{mag} (red lines). Details of fitting are given in the text.
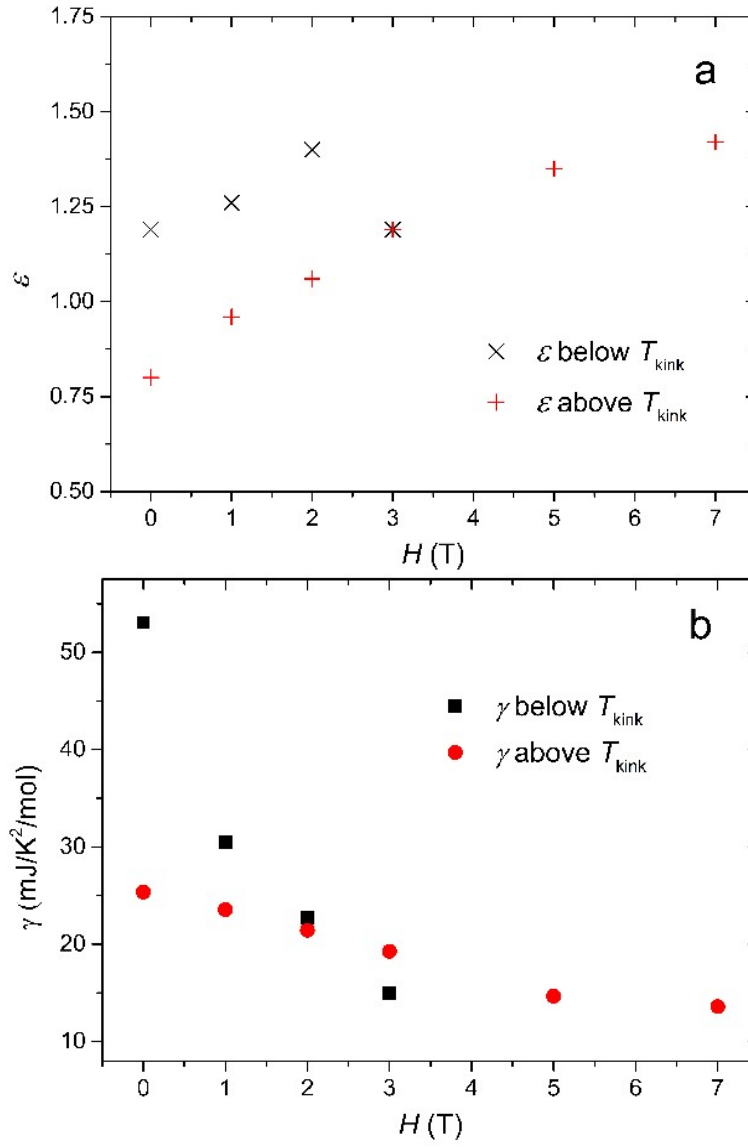
Fig. S7. Field dependences of ε (a) and γ (b) values extracted from the specific heat data below and above T_{kink}.
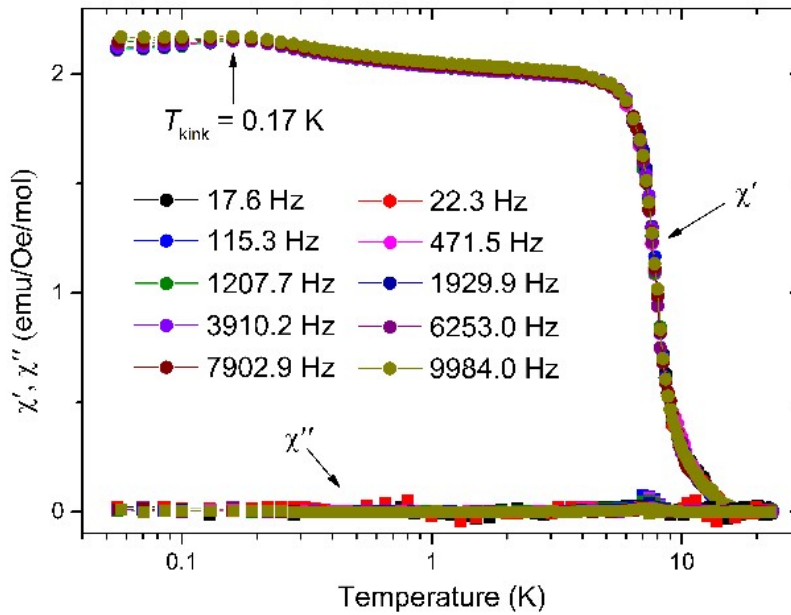
Fig. S8. χ' and χ'' vs T curves measured with various frequencies in the temperature range of 0.055 to 23 K. There is no obvious frequency dependence above 0.17 K. The real part χ' increases monotonically as temperature decreases and levels off below 5 K. Although χ' drops a little below 0.17 K, there is still large susceptibility towards 0 K, indicating substantial low-energy excitations. The peak temperature of the maxima at 0.17 K is not field-dependent. The imaginary part χ'' is much smaller than χ' and the χ'' vs T curve is basically flat.
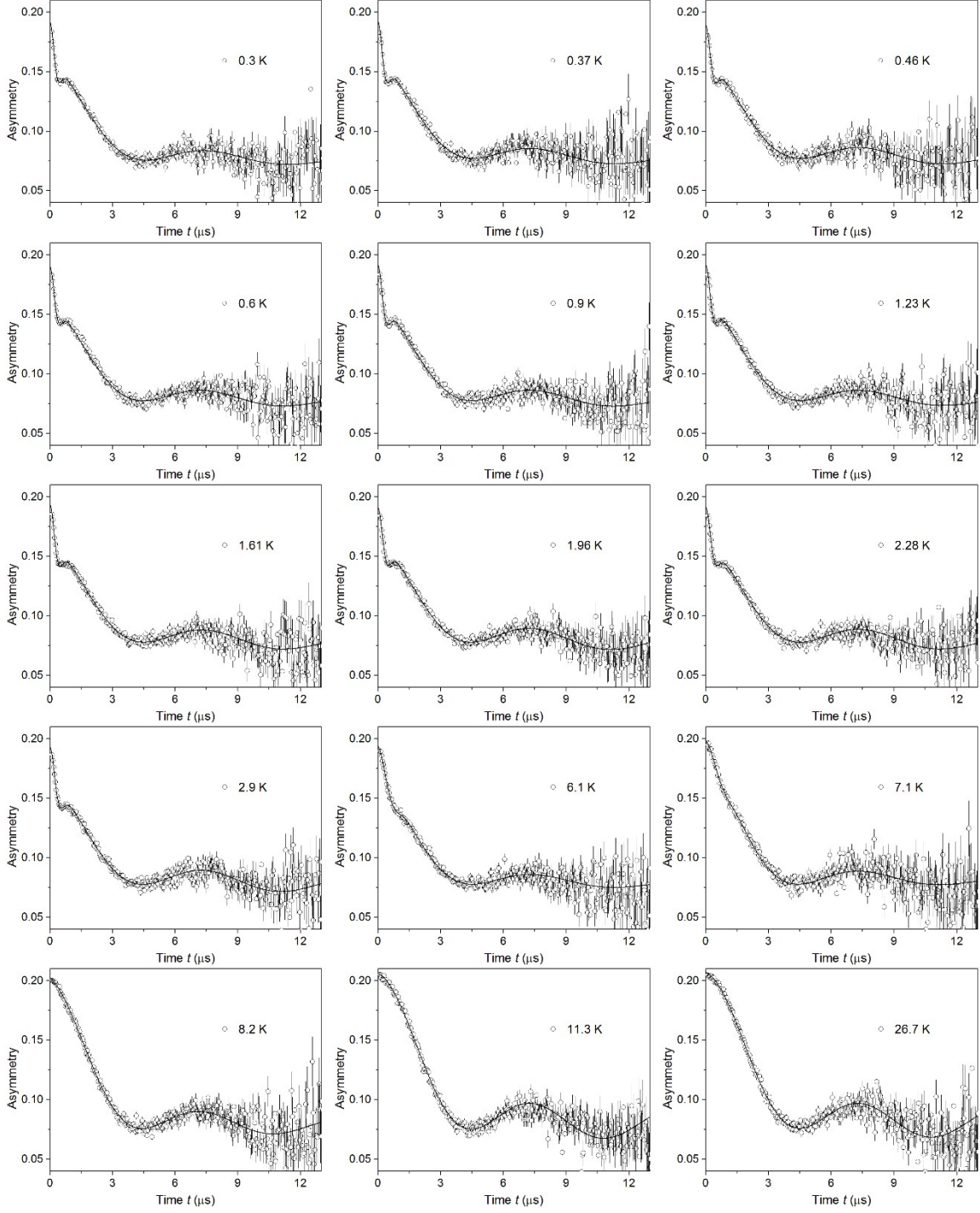
Fig. S9. Zero-field μSR time spectra measured at various temperatures from 0.3 to 26.7 K on S1, J-PARC. The solid lines are the best fits in terms of Eq. 2 as described in the text.

Table S1. Crystallographic information of **1**.

Compound	Cs(chrysene$^{•-}$)(THF)$_{0.5}$·(THF)$_{0.25}$ (**1**)
Empirical formula	C$_{84}$H$_{72}$Cs$_4$O$_3$
Formula weight	1661.09
Crystal system	Triclinic
Space group	$p\bar{1}$
a /Å	12.3931(3)
b /Å	13.0388(3)
c /Å	22.2180(7)
α/°	75.614(2)
γ/°	85.704(2)
β/°	77.205(2)
V/Å^3	3390.55(16)
ρ_{calcd}/g cm^{-3}	1.624
λ (Mo Kα)/Å	0.71013
μ/mm−1	2.184
T/K	90(2)
F (000)	1634
2ϑ range for data collection/°	4.3440−56.1640
Index ranges	−15<h<15, −16<k<9, −28<l<29
No. of measured reflections	13060
R_{int}	0.022
No. of refined parameters	820
No. of observed reflections, I > 2$\sigma(I)$	11672
Goodness-of-fit on F^2, S	1.057
R_1 [a], wR_2 [b] [I > 2$\sigma(I)$]	0.0516, 0.1393
R_1 [a], wR_2 [b] (all data)	0.0578, 0.1347

[a] $R_1 = [\Sigma||F_o| − |F_c||/\Sigma|F_o|]$. [b] $wR_2 = [\Sigma w(F_o^2 − F_c^2)^2/\Sigma w(F_o^2)^2]^{1/2}$.

Table S2. The assignments of vibrational mode of Raman spectra for pristine and compound **1**.

| Pristine Chrysene	Compound **1**	Assignment
293 (w)	286 (w)	CCC ring deformations
386 (w)	374 (m)	
480 (w)	470 (w)	
568 (s)	561 (w)	Out of plane of aromatic ring
680 (m)	666 (w)	
760 (m)	749 (w)	
880 (w) 1019 (w) 1044 (w) – 1183 (w)	863 (w) 998 (w) 1034 (w) 1067 (m) 1159 (w)	C–H in-plane deformation vibrations Out of plane C–H bending vibration
–	1193 (w)	C–C stretching
–	1224 (w)	C–C stretching
1332 (w)	1309 (w)	
1383 (s)	1350 (s)	Skeletal ring vibration
1434 (m)	1415 (w)	C=C stretching vibration
1576 (w)	1562 (w)	C=C stretching vibration
1622 (w)	1601 (w)	
w= weak; m= medium; s= strong		

References

1. J. Mesot, S. Janssen, L. Holitzner, R. Hempelmann, Focus: Project of a space and time focussing time-of-flight spectrometer for cold neutrons at the Spallation Source SINQ of the Paul Scherrer Institute, *J. Neutron Res.* **3**, 293 (1996).

2. R. T. Azuah, L. R. Kneller, Y. Qiu, P. L. W. Tregenna-Piggott, C. M. Brown, J. R. D. Copley, R. M. Dimeo, Dave: A comprehensive software suite for the reduction, visualization, and analysis of low energy neutron spectroscopic data, *J. Res. Natl. Inst. Stan. Technol.* **114**, 341 (2009).

3. Y. Li, B. Pan, S. Li, W. Tong, L. Ling, Z. Yang, J. Wang, Z. Chen, Z. Wu and Q. Zhang, Gapless quantum spin liquid in the S = 1/2 anisotropic kagome antiferromagnet $ZnCu_3(OH)_6SO_4$, *New Journal of Physics* **16**, 093011 (2014).

4. S. Yamashita, Y. Nakazawa, M. Oguni, Y. Oshima, H. Nojiri, Y. Shimizu, K. Miyagawa, K. Kanoda, Thermodynamic properties of a spin-1/2 spin-liquid state in a κ-type organic salt. *Nature Phys.* **4**, 459–462 (2008).

Additional Notes

Inelastic neutron scattering (INS) measurements. A broad continuum of magnetic excitation in INS spectra can be a strong evidence for the existence of deconfined spinons in QSL. We have collected INS spectra from powders of **1** for external magnetic fields of 0 and 1 T at 80 mK on the time-of-flight spectrometer FOCUS, Paul Scherrer Institute.[1] The wavelength of the incident neutrons was 2.5 Å with an energy resolution of 0.88 meV (FWHM) at E = 0. A dilution cryostat was used. About 2.5 g of powders were sealed in a double-wall Cu cylinder can filled with Helium gas as the exchange gas. INS data were analyzed using the DAVE software.[2]

The spectrum for 0 T is shown in Fig. S6a. There is seemingly continuous excitation extending from the elastic line up to about 6 meV (≈69.6 K), reflecting the overall energy scale of the magnetic exchange, in reasonable agreement with $|\vartheta_{CW}|$ = 62.1 K. In Fig. S6a, the INS intensity between Q = 2.5 and 3.5 Å^{-1} is most likely due to the phonon contribution often observed in organic materials, and the spike-like feature at around Q = 0.7 Å^{-1} is due to the scattering from the sample environment. Therefore, only the INS intensity within the Q range of 1 – 2.4 Å^{-1} is integrated and plotted as a function of the energy transfer E, as shown in Fig. S6b. Although the INS signal is quite weak and affected by the incoherent scattering of H atoms, a broad continuum between E = 2.2 and 7.6 meV can be seen and shows a clear magnetic-field dependence, indicating that it is of magnetic origin and may arise from the gapless excitation of spinons as expected in QSL. However, we cannot preclude the effect of strong incoherent scattering from H atoms on the INS signal due to the difficulty of deuteration. The strong phonon contribution and the weak magnetic INS signal (S = 1/2) also pose challenges for a clear identification of the magnetic excitation continuum.
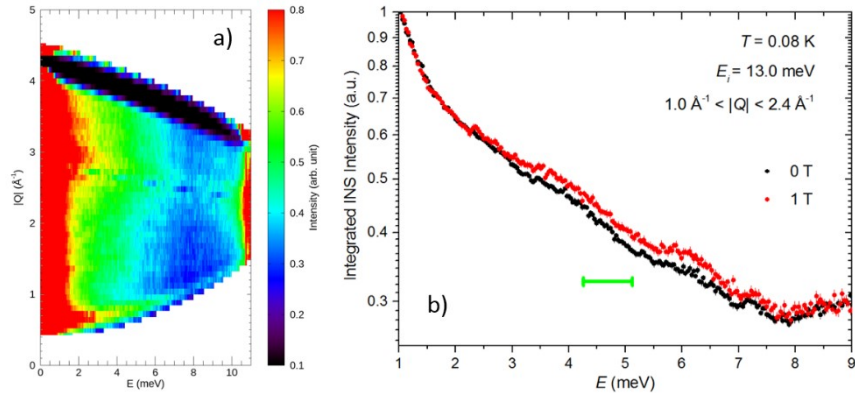
Inelastic neutron scattering (INS) spectra of **1**. a) INS spectrum for 0 T at 0.08 K. A broad continuum extends from the elastic line to about 6 meV, in agreement with $|\vartheta_{CW}|$ = 62.1 K. The INS intensity is integrated over the Q range of 1.0 – 2.4 Å^{-1} to avoid the phonon and the sample environment contributions. b) Integrated INS intensity plotted as a function of the neutron energy transfer E. The INS data for 0 and 1 T were obtained at 0.08 K with

an incident neutron energy of 13.0 meV. The green bar represents the instrumental resolution. The broad continuum is clearly affected by the application of an external magnetic field.